Hindawi
Geofluids
Volume 2023, Article ID 8102826, 12 pages
https://doi.org/10.1155/2023/8102826

Research Article

Insights into the Process of Gas Release from Organic-Rich Shale: Release Characteristics and Controlling Factors

Fei Li,[1] Wei Dang,[1,2] Fengqin Wang,[1,2] Haikuan Nie,[3] Yubo Feng,[1] Qiubo Liu,[4] Jiangtao Sun,[1] and Yao Ma[5]

[1]*School of Earth Sciences and Engineering, Xi'an Shiyou University, Xi'an 710065, China*
[2]*Key Laboratory of Tight Oil and Gas Geology of National Petroleum and Chemical Industry, Xi'an Shiyou University, Xi'an 710065, China*
[3]*Petroleum Exploration and Production Research Institute, SINOPEC, Beijing 100083, China*
[4]*No. 3 Oil Production Plant, PetroChina Changqing Oil Field Company, Qingyang 745400, China*
[5]*No. 5 Gas Production Plant, PetroChina Changqing Oil Field Company, Xi'an 710018, China*

Correspondence should be addressed to Wei Dang; dangw@xsyu.edu.cn and Haikuan Nie; niehk.syky@sinopec.com

Received 21 April 2022; Revised 6 November 2022; Accepted 15 February 2023; Published 11 May 2023

Academic Editor: Muhammad Tayyab Naseer

Shale gas release in canister can significantly enrich our understanding in gas-in-place characteristics. However, studies on shale gas release characteristics and its controlling factors are rare. In this study, gas release curves of 52 shale samples and 3 coal samples were measured using wellsite canister testing technique. According to curve shape, three curve patterns including L-shaped, S-shaped, and M-shaped are identified, and the difference among three curve patterns mainly lies in the fractional gas volume released in surface temperature stage. To evaluate the dependence of released gas content on shale properties, the variation in released gas content with organic matter, minerals, porosity, permeability, specific surface area, and pore volume is analyzed and found that the released gas content shows a strong dependence on the properties that control or could increase gas adsorption and diffusion capacity, such as TOC content, specific surface area, and permeability, while showing no dependence on the properties that control free gas storage capacity, such as minerals, porosity, and pore volume. Additionally, correlations of released gas content with adsorbed/free gas show that the released gas during canister testing is the gas that was in the adsorbed state in reservoir, and the free gas has been lost during coring, as well as a fraction of adsorbed gas. Above findings provide insightful information not only on gas-in-place evaluations but also on the dynamic behavior of adsorbed/free gas from producing well.

1. Introduction

The successful development and production of shale gas in the US greatly stimulated other countries (e.g., Canada, China, Australia, and Poland) to explore and investigate the gas potential of organic-rich shales [1–8]. During exploration and investigation, the gas content, which is referred to the amount of gas that is stored within shale reservoir, is very important to evaluate the gas potential and commerciality of shale gas plays [9] and, therefore, must be understood and evaluated. With regard to this, a gas release measurement technique called wellsite canister testing has been adopted to measure the shale gas content and compositions (e.g., methane, ethane, nitrogen, carbon dioxide, and hydrogen) in recent years [10–14]. Here, we use the term "gas release" instead of "gas desorption," and the main reason is that gas production from shale is the outcome of several different types of gas release process, including, but not limited to, desorption, and the gas release process should in fact be referred to "release" in order to encompass all forms of gas release process during canister testing [15, 16].

In canister testing, the gas is initially allowed to release from retrieval shale core samples, and the release curve of gas volume versus time is measured. Such release curves provide insightful information not only on gas content estimation [14, 17, 18] but also on rock petrophysical and gas

diffusion properties [19–21]. However, because of high expense and time consuming of wellsite canister testing, isothermal adsorption, and other basic experiments, there is paucity of published data investigating the shale gas release characteristics and its controlling factors; moreover, its importance on gas-in-place evaluations has not been fully evaluated and understood. Javadpour et al. [15] conducted canister testing on shale and coal samples and observed that the gas release curve in shale is different from that in coal. They also found that the shale gas release curve can be divided into four sections, and each section of the curve represents a specified type of gas flow. Vasilache [22] reported two abnormal gas release curves of shale samples and found that the gas generation caused by anaerobic bacterial growth during canister testing is the main reason for this phenomenon. Tang et al. [23] stated that the shapes of gas release curves vary significantly among different shales. Recently, Gao et al. [24] studied the shale gas release process by using canister testing and gas chromatograph technique. They found that the release process of shale gas was controlled by gas flow behavior in shale matrix. Dang et al. [25] reported their preliminary findings on shale gas evolution during canister desorption.

Some of above studies also discussed the dependence of shale gas release on temperature and organic matters. For example, Tang et al. [23] and Xiong et al. [26] found that both released gas volume and gas release rate at high temperature stage is greater than that at reservoir temperature stage. However, Liu et al. [27] observed the opposite phenomenon. The organic matter, which possess high gas adsorption capacity [28, 29], has a significant effect on shale gas release characteristics. Firstly, the higher the total organic carbon (TOC) content, the higher the gas volume released from shales [26]. Secondly, the higher TOC content, the weaker the gas desorption capability [30]. Unlike coals that gas released from which during canister testing is mainly from adsorbed gas [31], or conventional reservoir that gas released from which is mainly from free gas, both free gas and adsorbed gas will release over time during shale gas release and production [3], but at different rates and stages [32, 33].

As mentioned, research on characteristics of gas release in shale and their interactions with shale properties is not well established, and its importance on gas-in-place evaluations has not been fully evaluated and understood. In this study, an effort has been made to observe gas release characteristics estimated directly from wellsite canister testing, and then, the occurrence state of released gas is discussed along with the methane adsorption capacity. Finally, the dependence of released gas content and gas release rate on shale matrix and temperature is discussed.

2. Samples and Methods

2.1. Core Samples. Freshly drilled 52 shale core samples and 3 coal core samples from the southern North China Basin were put into canister immediately upon core retrieval. All the drilled shale samples were obtained by conventional coring from the depth of 2800~3000 m, and the length of core samples that were selected for canister testing mainly ranges from 20 cm to 30 cm. Figure 1 shows basic geological and sampling information of core samples, including lithology and sampling depth. Among these core samples, the detailed discussion on geochemical, mineralogical, petrophysical, and pore structure of 35 shale samples was already mentioned in previous report [34], and the rest of 17 shale samples and 3 coal samples are newly introduced here. The detailed information including these samples is reproduced and provided in the Supplementary Material (Table S1).

2.2. Methods

2.2.1. Wellsite Canister Testing. In this study, our homemade canister testing instrument was used at the wellsite of Mouye-1 well to measure the gas release data (Figure 2). The information on overall designing and individual components of this instrument, instrument parameters, and experimental procedures can be found in the author's recent published article [10]. It should be noted that the gas release data were measured at two temperature stages in this study to fully understand the gas release process and characteristics: surface temperature stage of 10°C and reservoir temperature stage of 80°C. After manually recording the gas release volume data over time, the gas release curves were plotted with the cumulative time in the X-axis and the cumulative gas release volume in the Y-axis, and the released gas content, which is traditionally referred to "desorbed gas content" in canister testing, was obtained (Table S1). In order to improve comparative study, the gas release curves are normalized and are expressed in terms of fractional release volume, as a function of time t:

$$Q_{\text{fractional}}(t) = \frac{Q_{(t)}}{Q_{\infty}}, \tag{1}$$

where $Q_{(t)}$ is the cumulative gas release volume at time t and Q_{∞} is the total gas release volume.

2.2.2. In Situ Shale Gas Content. It is well known that the hydrocarbons existed in adsorbed, free, or dissolved state in shale matrix [3, 35], and the in situ gas content can be calculated by summing up above three components. In this work, the dissolved gas was neglected because of the thermal cracking (thermal maturity of 3.34% on average) of liquid hydrocarbons in shale matrix [34]. Therefore, only adsorbed gas and free gas were considered to quantify in situ shale gas content:

(1) Adsorbed gas: the gas accumulated on the surface area of organic and inorganic matters, and its volume can be quantified from the adsorption isotherm measurements. In here, a volumetric apparatus was applied to measure the methane adsorption isotherms at temperatures of 80°C. The detailed information about apparatus components and experimental procedures can be found in previous literatures [36–38]. Although the experimental pressure range is not enough to indicate the subsurface pressure conditions of shale reservoir, the methane adsorption capacity at reservoir pressure can still be produced by correlating the methane adsorption isotherms with the Langmuir model [39], giving

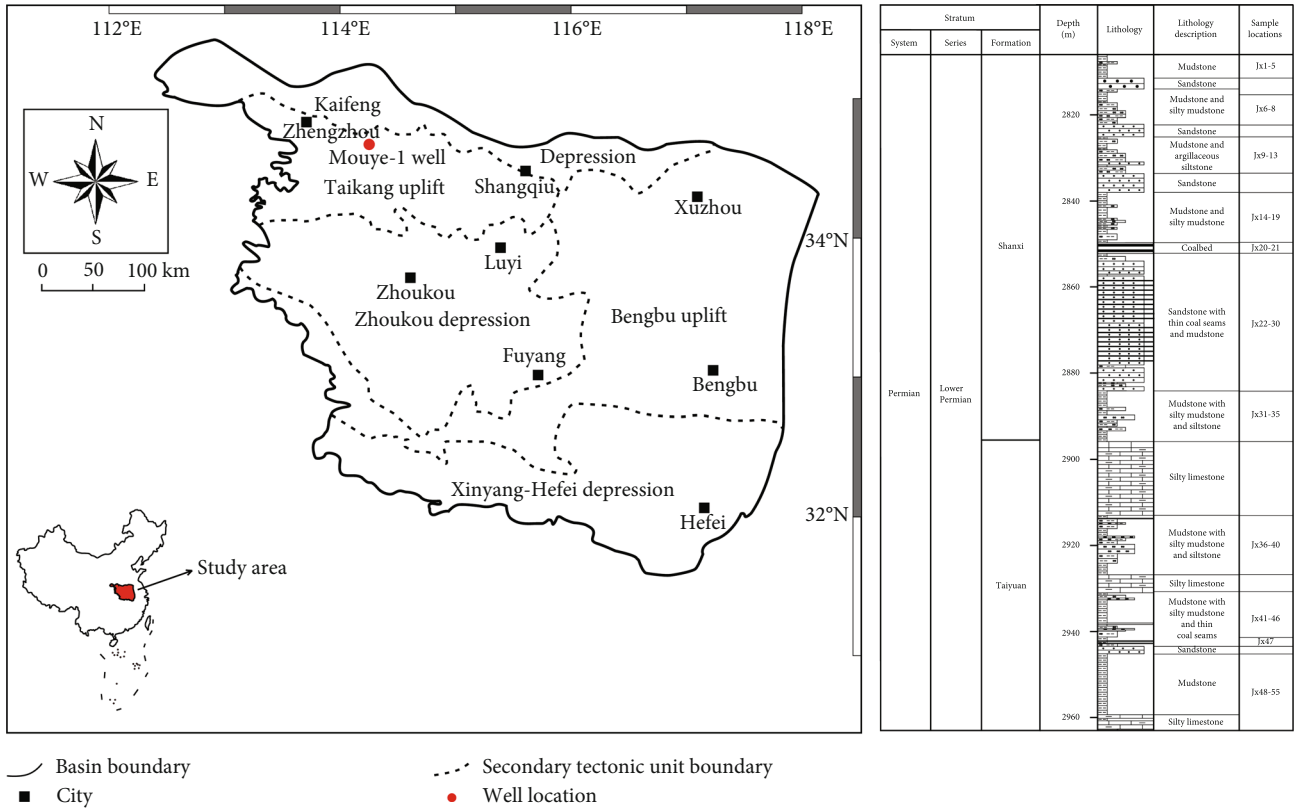

Figure 1: Location and lithological column of the sampling well—Mouye-1 well (modified from Dang et al. [52]).

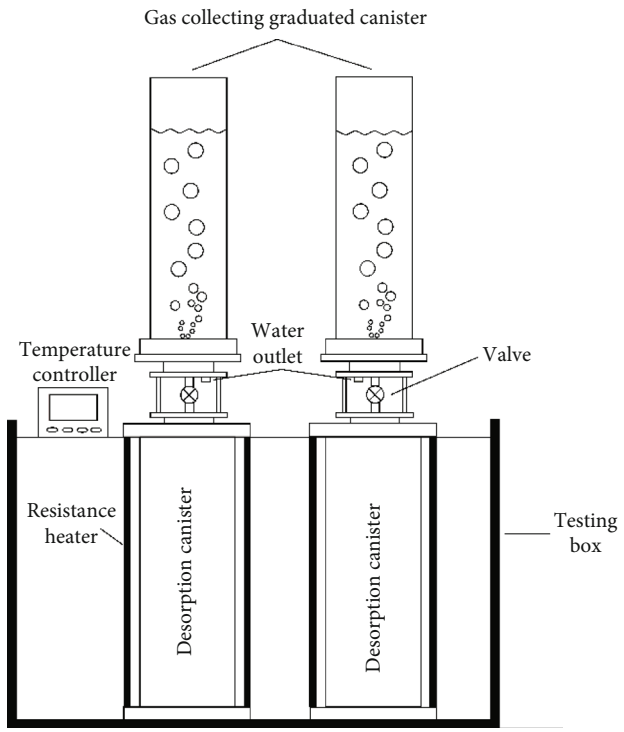

Figure 2: The canister testing instrument for gas release measurement [10].

$$V_a = V_L \frac{P}{P_L + P}, \tag{2}$$

where V_a is adsorbed gas volume in ml/g, V_L is the Langmuir volume in ml/g, P_L is the Langmuir pressure in MPa, and P is the experimental pressure in MPa

(2) Free gas: the gas accumulated in the pore or microfracture space in the compressed state, and its volume can be quantified using the method by Ambrose et al. [40], giving

$$V_f = \frac{1}{B_g}\left[\frac{\varnothing \bullet S_g}{\rho} - \frac{1.318 \times 10^{-6}\bar{M}}{\rho_s}\left(V_L \frac{P}{P_L + P}\right)\right], \tag{3}$$

where V_f is free gas volume in ml/g, $\varnothing$ is total porosity (dimensionless), S_g is gas saturation with a value of 0.3 for Shanxi shales and 0.4 for Taiyuan shales [41] (dimensionless), ρ is density of bulk rock in t/m^3, ρ_s is adsorbed gas density in t/m^3 with a value of 0.37 [40], $\bar{M}$ is apparent methane molecular weight, and B_g is gas volume factor and was obtained from the following equation:

$$B_g = \frac{P_s}{Z_s(T_s + 273.15)} \times \frac{Z(T + 273.15)}{P}, \tag{4}$$

where P_s is standard pressure with a value of 0.1 MPa, Z_s is gas compressibility factor under standard temperature and

pressure conditions with a value of 1, T_s is standard temperature with a value of 0°C, Z is gas compressibility factor under reservoir condition (80°C and 28 MPa), P is reservoir pressure in MPa, and T is reservoir temperature in °C

2.2.3. Total Organic Carbon Content. The total organic carbon (TOC) was determined using a Leco CS230 carbon/sulfur analyzer. Samples were first crushed to powder with a particle size < 100 mesh. Excess dilute hydrochloric acid was used to remove carbonates from the measured samples. After rinsing and drying, decarbonated samples were reweighed and combusted at high temperatures in the Leco CS230. We compared unknown samples to a standard value to compute the organic carbon content of each sample (in weight percent).

2.2.4. Mineral Compositions. Mineral compositions were determined by X-ray diffraction (XRD) on a Bruker D8 Discover X-ray diffractometer. The experiment consists of two independent procedures. First, the total clay content was determined by analyzing the bulk mineral composition of the powdered sample finer than 10 μm. Then, the individual clay mineral contents of the fraction finer than 2 μm were determined.

2.2.5. Nitrogen Adsorption. In order to qualitatively and quantitatively characterize the pore structure, nitrogen adsorption experiments were carried out. The shale samples involved in this study were manually pulverized and sieved into particles of about 80 mesh size, dried in a vacuum oven at 90°C overnight, and degassed at 90°C for 12 hours to remove moisture and residual gas. Then, N_2 adsorption at -196.15°C was carried out on a Quantachrome Autosorb gas adsorption system over the relative pressure of 0.005~0.995, and the adsorption isotherms were established. Finally, the BET and BJH methods were used to extract the specific surface area and the pore volume from the adsorption isotherms.

2.2.6. Porosity and Permeability. The porosity of the shale samples was measured using the UltraPore-200A porosimeter, and the permeability of the shale samples was measured using the Ultra-Perm 200 permeameter. These measurements were performed at 23°C and 1025 hPa.

3. Results and Discussions

3.1. Shale Gas Release Characteristics in Canister. Using the wellsite canister testing method, the normalized gas release curves of all 52 shale samples and 3 coal samples (samples JX20, JX21, and JX47) were measured and are shown in the Supplementary Material (Figure S1-S2). It can be observed that the shape of these gas release curves is different among each other, but some phenomenon in common can still be observed. Thus, for better understanding and comparison study of shale gas release curve, three typical release curve patterns including L-shaped curve pattern, S-shaped curve pattern, and M-shaped curve pattern are identified (Figure 3), and the characteristics of each pattern are summarized as follows:

(1) L-shaped curve pattern is the most common gas release curve in measured shale samples (Figure 3(a)). In the surface temperature stage, the gas volume released from shale samples is close to zero, and the release curve is close to a straight line. During the reservoir temperature stage, the gas volume released from shale samples increased steeply and then flatten to a plateau

(2) S-shaped curve pattern is another most common gas release curve in measured shale samples (Figure 3(b)) and one coal sample of JX47. In this kind of pattern, a small fraction (no more than 0.2, at most) of the total gas released from shale samples in surface temperature stage, forming the first plateau, and with the surface temperature increased to reservoir temperature, the gas volume increased significantly and then flatten to form the second plateau

(3) M-shaped curve pattern is observed in one shale sample of JX30 and two coal samples of JX20 and JX21 (Figure 3(c)). In this kind of pattern, the gas volume released in surface temperature stage is comparable to that in reservoir temperature stage, and the gas release curves of two temperature stages share similar trends, with gas volume first increased significantly and then flatten to plateau.

By comparing, we found that the difference among three curve patterns mainly lies in the fractional gas volume released in surface temperature stage (S1) and the fractional gas volume released under reservoir temperature of 80°C (S2). It can be observed from Figure 4 that the M-shaped curve pattern has the highest released gas content, at 17.22 m^3/t on average, followed by S-shaped curve pattern, at 1.72 m^3/t, and the L-shaped curve pattern has the least released gas content with an average value of 0.51 m^3/t. Considering the distribution consistency between fraction of S1 and released gas content, therefore, the released gas content may possess a significant effect on the fraction of S1. It should be noted that the sample of JX47 is an exception. Although the sample of JX47 has the highest gas content of 27.80 m^3/t, its S1 value is still low. The cause for this phenomenon may be due to the lithology. Compared to the coal samples of JX20 and JX21, the gas adsorption capacity of sample JX47, which is muddy coal, is weaker. So, some adsorbed gas, which should had been released at surface temperature stage, has lost before the sample was sealed in canister, making the S1 low.

3.2. Understanding the Occurrence State of Released Gas in Canister. The occurrence state of released gas is of great significance in evaluating the gas-in-place characteristics and gas production behavior but has not been fully understood and evaluated. By using the methods in Section 2.2, the adsorbed gas content of 33 shale samples was obtained from the isotherms (Figure 5) and is listed in Table S1 along with the free gas content.

In Figure 6, the variation in released gas content with adsorbed and free gas contents is plotted. It can be observed

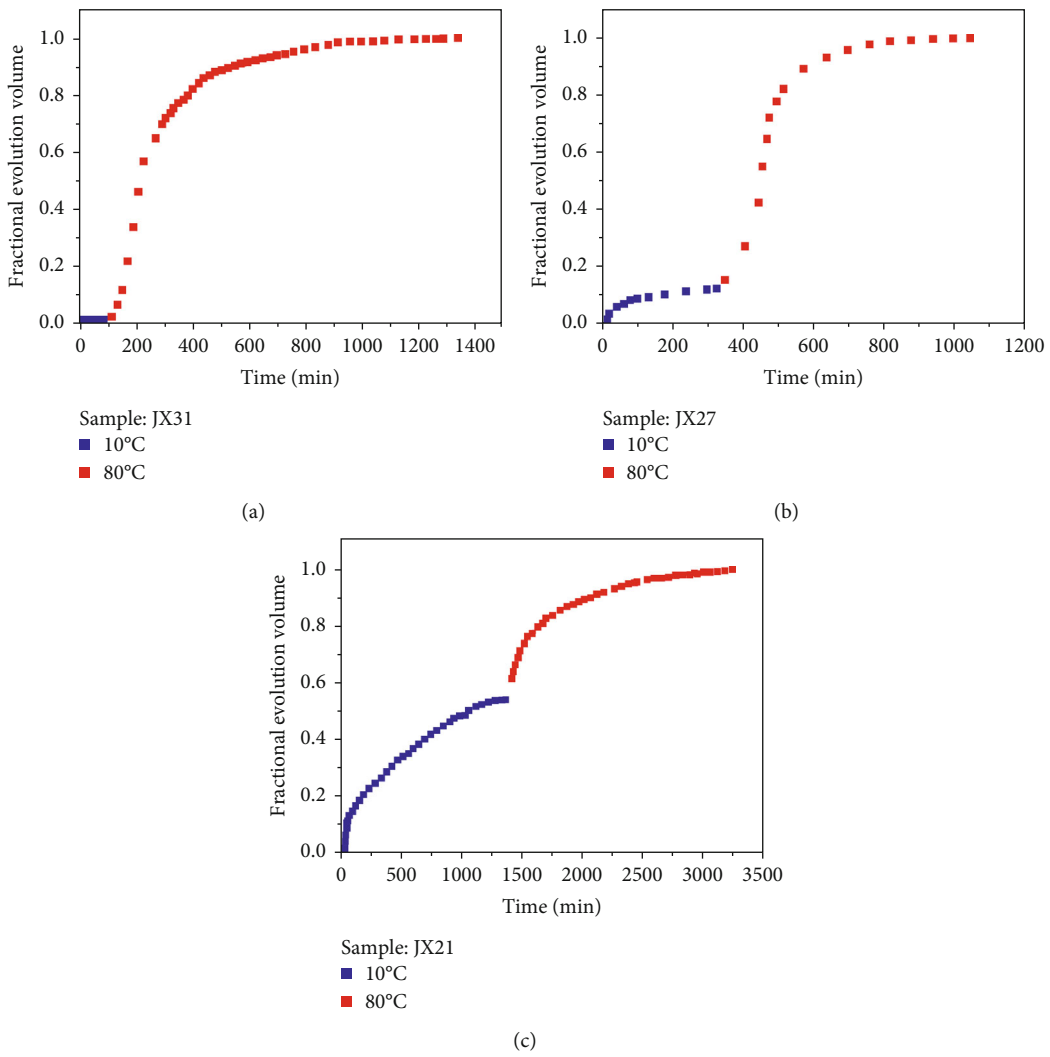

Figure 3: Typical gas release curves of shale gas and coalbed methane: (a) L-shaped curve with one plateau, (b) S-shaped curve with two plateaus, and (c) M-shaped curve.

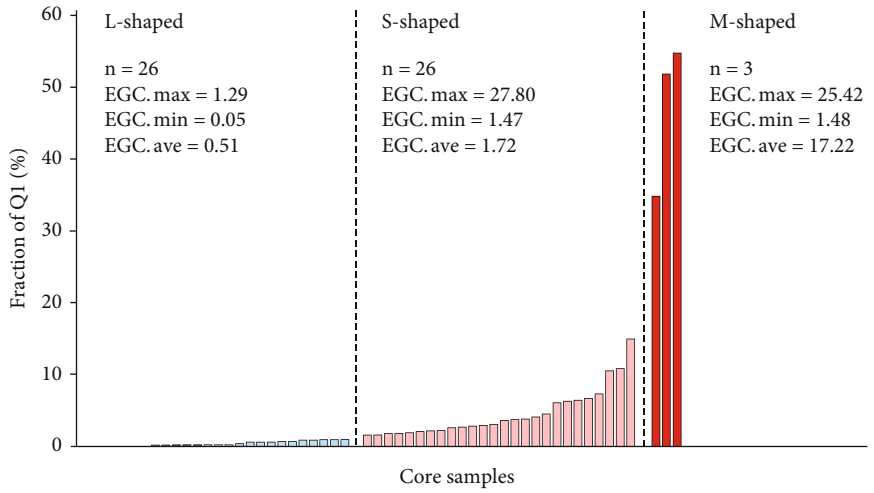

Figure 4: Histogram of fraction of S1 for core samples based on different curve patterns. EGC.max: maximum released gas content; EGC.min: minimum released gas content; EGC.ave: average released gas content.

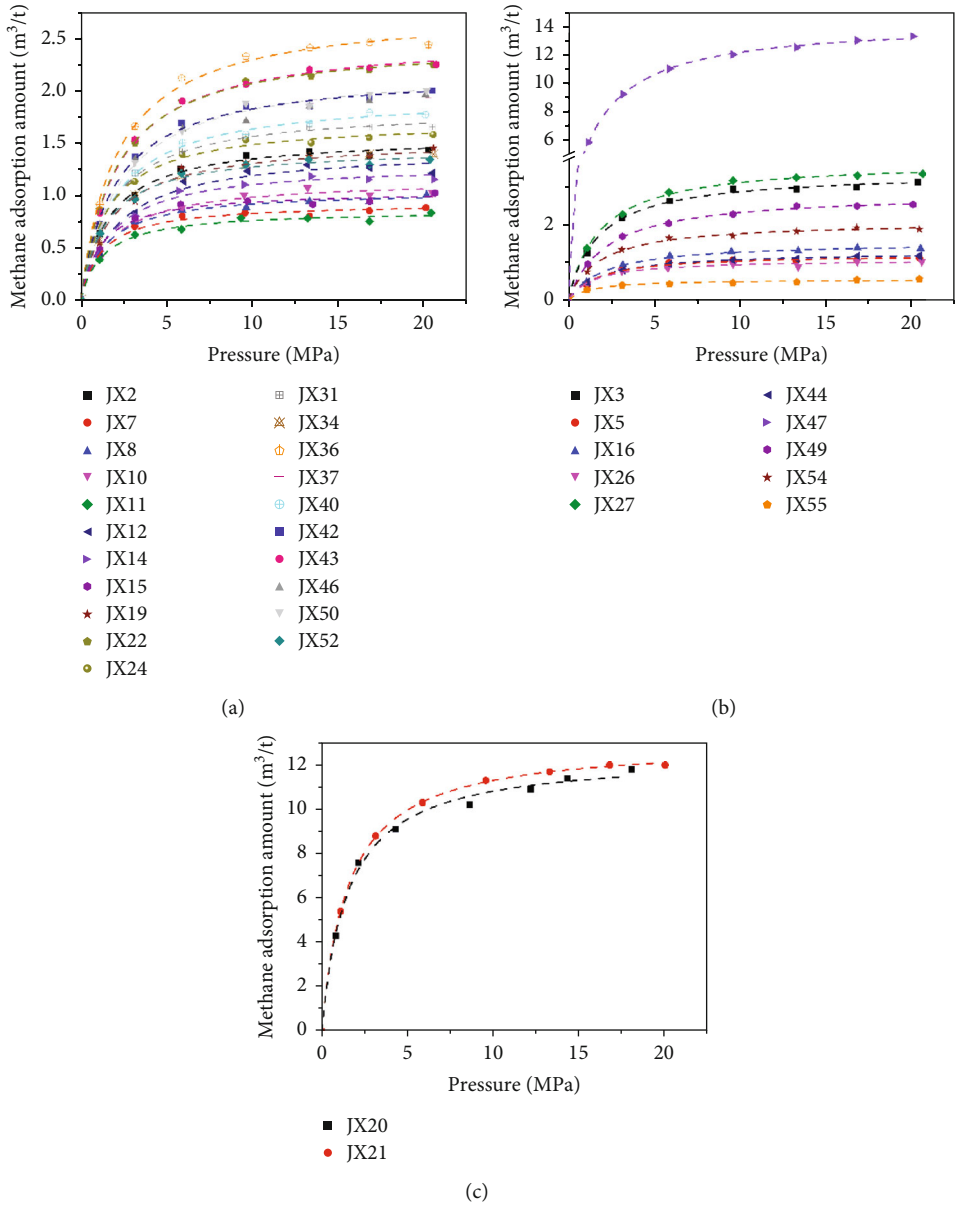

Figure 5: Absolute methane adsorption isotherms of shale and coal samples: (a) L-shaped samples, (b) S-shaped samples, and (c) M-shaped samples.

that there is an excellent positive correlation of released gas content with adsorbed gas content (Figure 6(a)), while there is no obvious trend between released gas content and free gas content (Figure 6(b)), indicating that the released gas content during canister testing is significantly controlled by adsorbed gas, and the free gas does not affect evolve gas content. Additionally, we observed in Figure 6(a) that all values fall below the solid line of "released gas content is equal to methane adsorption capacity," indicating the released gas during canister testing is the gas that was in the adsorbed state in reservoir, and a fraction of adsorbed gas has been lost during coring in addition to free gas. This finding contrasts the results of Bustin et al. [42] that documented the "desorbed" gas content of the Barnett shales invariably exceeds the methane adsorption capacity and concluded that the "desorbed" gas captured substantial free gas in addition to adsorbed gas. Due to lacking basic information of shale samples in their report, the causes for two different observations have not been drawn but may lie in different shale properties and coring process. Additionally, Figure 6(a) shows another interesting phenomenon that the gap between the black line and the red fitting line shows a tendency to increase with increasing adsorption capacity, indicating that the greater the methane adsorption capacity, the more the loss of adsorbed gas during coring. Upscaling from core data to field production, this phenomenon may improve our understanding in the production behavior of adsorbed gas. However, the reasons for this phenomenon are so far not understood, and additional measurements are required to confirm.

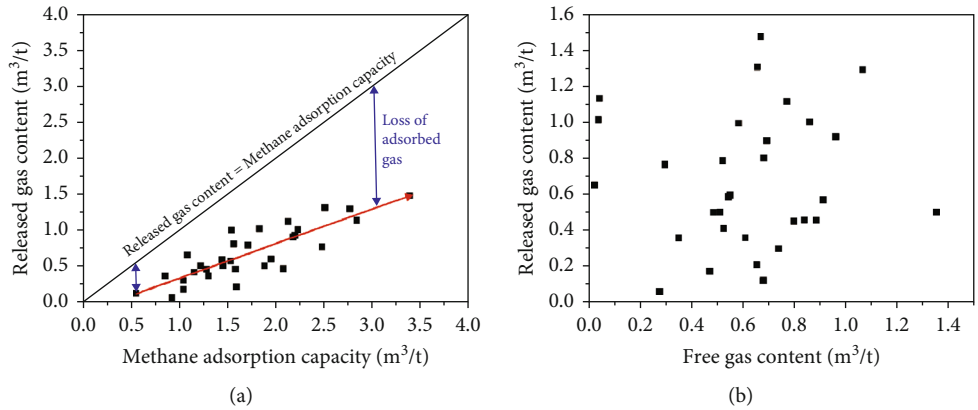

Figure 6: Variation in released gas content with (a) methane adsorption capacity and (b) free gas content. The solid line is an upper limit of gas content released from adsorbed gas. Values falling below the solid line indicate that the released gas during canister testing is the gas that was in the adsorbed state in reservoir.

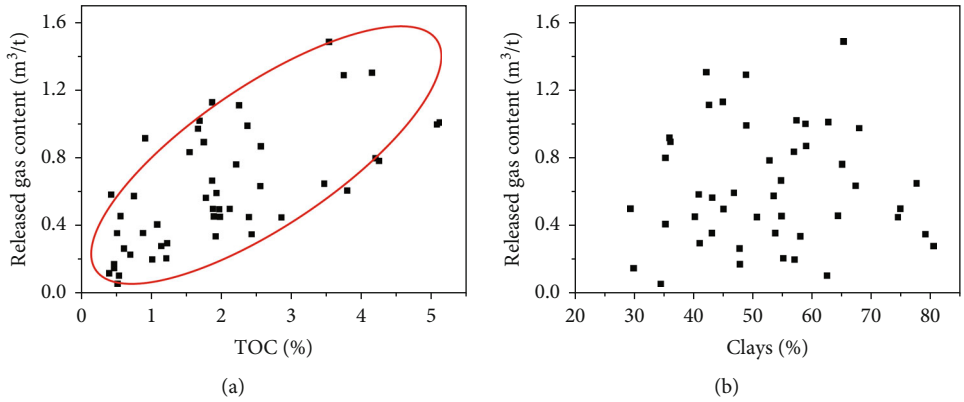

Figure 7: Variation in released gas content with (a) TOC and (b) clays.

3.3. Dependence of the Released Gas Content on Shale Matrix and Temperature

3.3.1. Organic and Inorganic Compositions. Considering the effect of organic matter and clay minerals on shale gas storage capacity [43–45], the dependence of which on organic and inorganic compositions is also important but is not well evaluated. To this end, the shale samples were analyzed in detail with respect to variations in released gas content as a function of TOC and clays. Results of these evaluations are given in Figure 7.

As expected, there is a good positive correlation of released gas content with TOC content (Figure 7(a)), indicating that the released gas content increased with increasing TOC, and this positive correlation may be attributed to high methane adsorption capacity and strong adsorption force of organic matter [46]. Xiong et al. [26] and Shi et al. [47] observed similar effects of increasing released gas content with increasing TOC. They concluded that the organic matter offers more specific surface area and total porosities for methane molecule, resulting in a positive effect on released gas content. Tang et al. [30] performed a similar set of experiments and found that the adsorption phenomenon caused by organic matter makes it difficult for methane to migrate out of shale matrix due to high methane adsorption capacity, and therefore, few adsorbed gas lost during coring. This effect is confirmed by investigations by Schloemer and Krooss [48]. They found that the physical interactions that occur between methane molecule and organic matter could restrict the mobility of methane molecule.

Given the positive effect of clays on methane adsorption capacity [43], it is quite unexpected that no specific trend is observed between released gas content and clays in this study (Figure 7(b)). Additionally, because of the complementary relationship between clays and brittle minerals, no correlation is observed between released gas content and brittle minerals as well (not shown), indicating that minerals have no obvious effect on released gas content of shale. This phenomenon may be attributed to the role of inorganic minerals in adsorbed/free gas storage, and the free gas stored in pores (i.e., pores associated with clays and brittle minerals) has been totally released and lost before canister testing.

3.3.2. Effective Porosity and Permeability. Effective porosity and permeability are two of the most important and crucial properties to evaluate shale gas storage capacity and gas flow efficiency. To evaluate the dependence of released gas content on effective porosity and permeability, the effective porosity and permeability are plotted in Figures 8(a) and

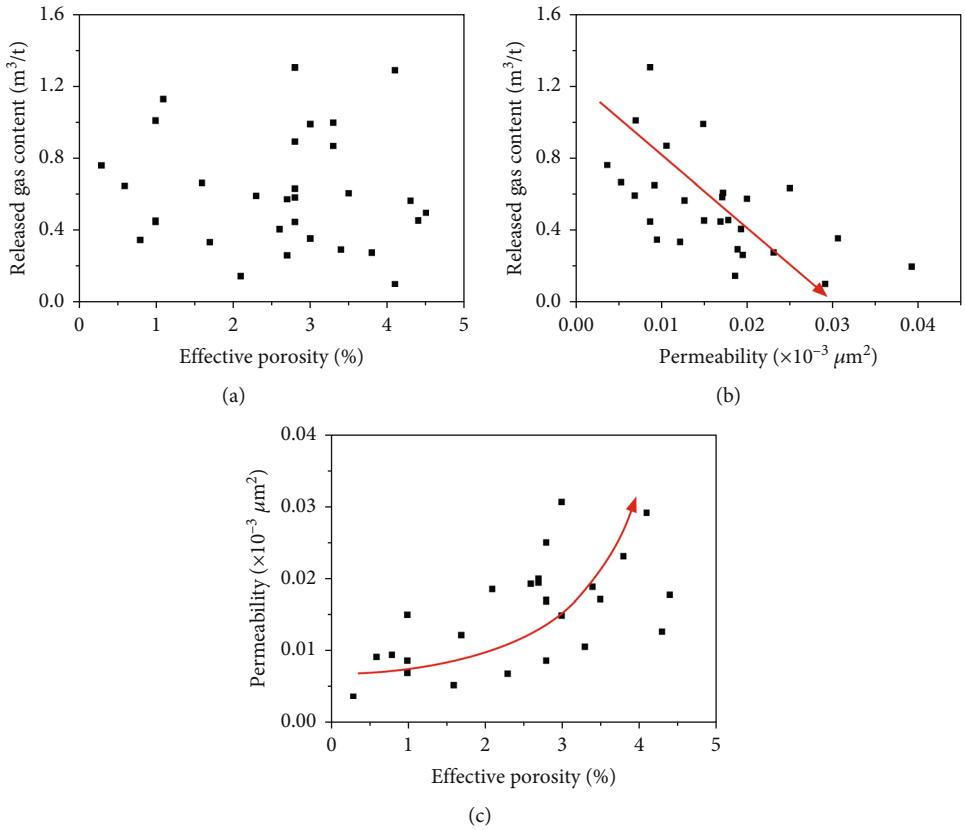

Figure 8: Variation in released gas content with (a) effective porosity and (b) permeability. (c) Variation in permeability with porosity.

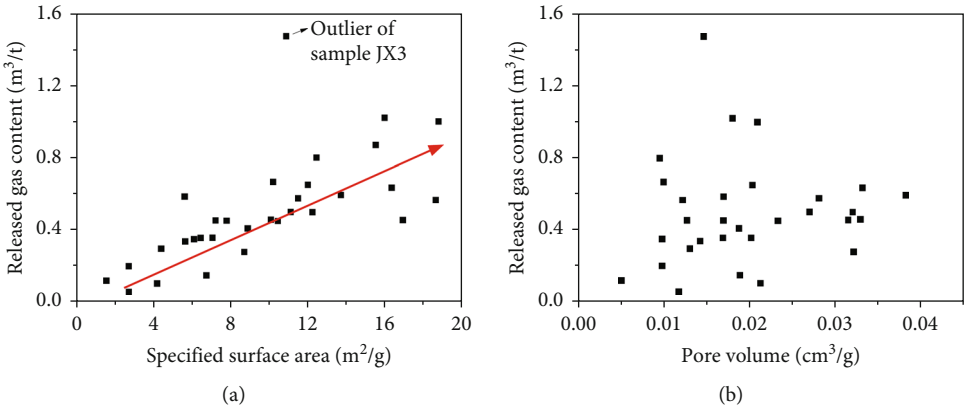

Figure 9: Variation in released gas content with (a) specific surface area and (b) pore volume.

8(b), respectively, as a function of released gas content. It can be observed that the released gas content did not show a trend with effective porosity, while showing a negative correlation with permeability, indicating that the free gas stored in pore space has been lost during coring, and moreover, the greater the permeability, the easier the gas lost during coring. In Figure 8(c), the variation in permeability with effective porosity is plotted, and a moderate positive correlation between effective porosity and permeability is observed. Because the connected pores are the primary space and channel by which gas flow through shale matrix, above permeability-porosity correlation is not surprising and indicates that the higher the porosity and permeability, the more and the easier it is for gas to flow out of shale matrix during coring and hence the fewer the gas left for canister testing.

3.3.3. Nanoscale Pore Properties. To evaluate the dependence of released gas content on nanoscale pore (<300 nm) properties, the variation in released gas content with specific surface area and pore volume is plotted in Figures 9(a) and 9(b), respectively. It can be observed that there is a good positive correlation of released gas content with specific surface area (Figure 9(a)), and this positive correlation may be

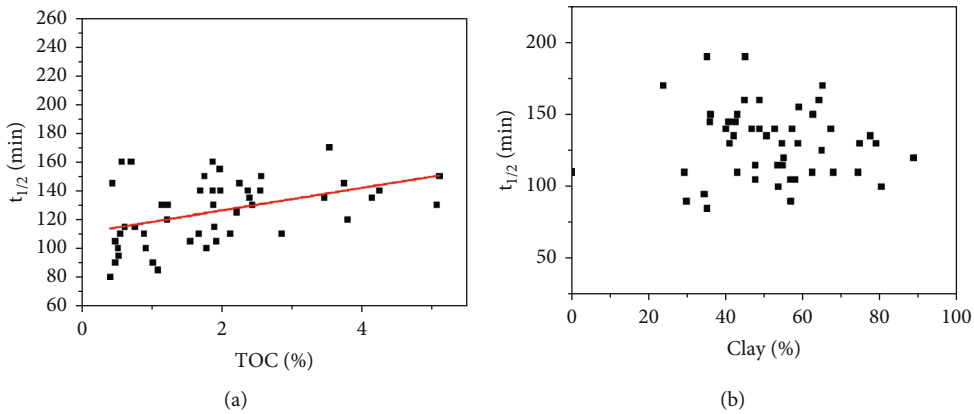

Figure 10: Variation in gas release rate with (a) TOC and (b) clay.

attributed to the positive correlation between specific surface area and adsorption capacity. The above observation is supported by Tang et al. [23], who performed shale gas canister release experiments at 90°C and found that the released gas content increased with increasing specific surface area. Additionally, they also documented a continuous and gradual increase of released gas content with total pore volume and concluded from their study that the pores in marine shale are favorable for adsorbed gas accumulation. In the present work, however, no obvious trend is observed between released gas content and pore volume (Figure 9(b)), indicating that the pores in transitional shale are favorable for free gas accumulation, instead of adsorbed gas. This preliminary conclusion can be furtherly supported by investigations by Yang et al. [49]. They concluded that the pores in transitional shale are not dominated by organic matter pores, but inorganic pores which have less adsorption capacity and are in favor of free gas storage.

3.3.4. Experimental Temperature. The significant effect of experimental temperature on shale gas release content can be clearly observed in Figure 3, indicating that the released gas content increased with increasing temperature. This phenomenon is also confirmed by investigations by Tang et al. [30] and Xiong et al. [26] and can be attributed to the negative effect of temperature on methane adsorption capacity and the positive effect of temperature on gas diffusion [50].

3.4. Dependence of the Gas Release Rate on Shale Matrix and Methane Adsorption Capacity

3.4.1. Organic and Inorganic Compositions. To quantitatively describe the rate of gas release, the half-life time $t_{1/2}$, which is the time required for a certain quantity of shale gas to reduce to half of its initial values, is used in this study. This value can be easily obtained from the desorption curve described in Figure 3 and Figure S1-S2.

In order to investigate the effect of organic and inorganic composition on the gas release rate, the variation in the $t_{1/2}$ versus the TOC content and clay is plotted in Figure 10. It can be seen from Figure 10(a) that the $t_{1/2}$ is positively correlated with the TOC content, i.e., the $t_{1/2}$ increases with an increase in the TOC content, indicating that the higher the TOC content, the slower the gas release rate. This correlation is anticipated, because the organic matter has strong gas adsorption capacity, making gas molecules difficult to desorb and transport. Additionally, the nonporous organic matter can occupy the micropore volume, prolonging gas diffusion length, and increasing diffusion resistance [51]. Compared to the TOC content, it is evident that the clay has no effect on the gas release rate (Figure 10(b)). Inorganic minerals act as storage in adsorption as well as in free gas, and the free gas stored in the pores has been completely released in the wellsite canister testing. So, the inorganic minerals (i.e., clay) have no effect on the gas release rate.

3.4.2. Effective Porosity and Permeability. In order to evaluate the dependence of gas release rate on effective porosity and permeability, the half-life time $t_{1/2}$ was plotted against the permeability and effective porosity, as shown in Figure 11. It is clear from Figure 11(a) that the $t_{1/2}$ decreases with an increase in permeability, indicating that the gas release rate is positively correlated with the permeability. However, there is no correlation between the $t_{1/2}$ and the effective porosity (Figure 11(b)), indicating that effective porosity has no obvious effect on the gas release rate. This phenomenon is also anticipated because the higher permeability indicates the better connectivity of micro porosity and cracks, which can shorten the transport time of gas from the pores and cracks to the outside of shale matrix and accelerate the gas release process.

3.4.3. Nanoscale Pore Properties. As the main occurrence space of shale gas, the pore properties may also affect the gas release rate. It is clear from Figure 12(a) that the values of the $t_{1/2}$ increase with an increase in specific surface area. This phenomenon may be caused by the strong interaction between the pore surface and gas molecules. Therefore, although the larger specific surface area could provide more adsorption sites and increase the methane adsorption capacity [28], it can also decrease the gas release rate as well as the gas production efficiency. Unlike the specific surface area, the $t_{1/2}$ has no

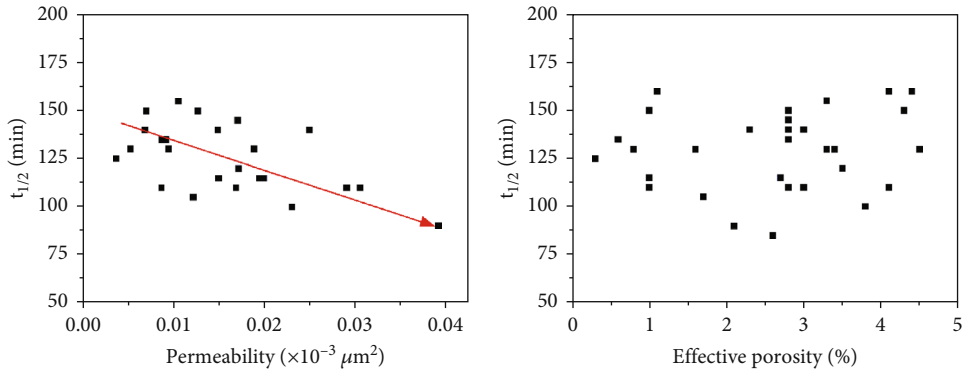

Figure 11: Variation in half-life time $t_{1/2}$ with (a) permeability and (b) effective porosity.

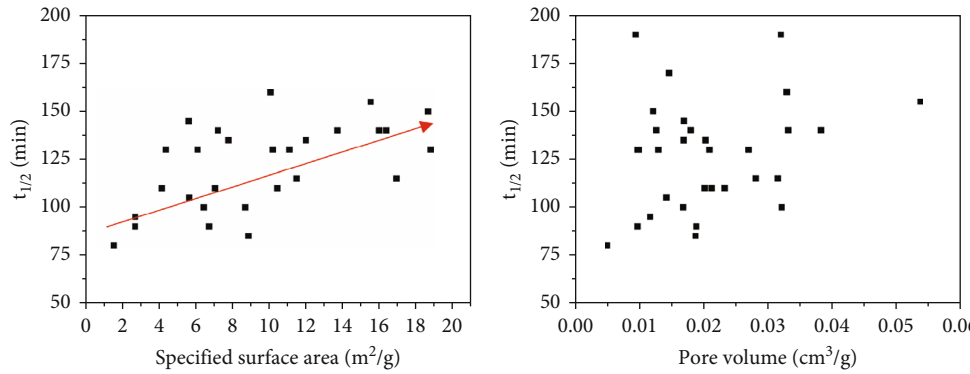

Figure 12: Variation in gas release rate with (a) specific surface area and (b) pore volume.

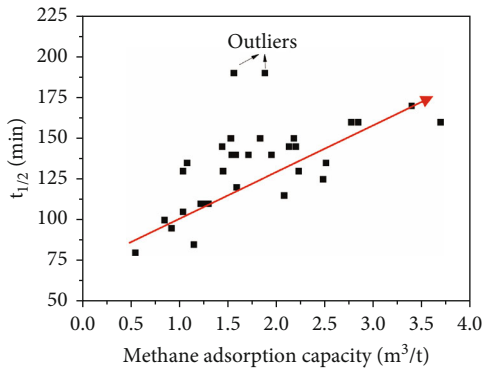

Figure 13: Variation in half-life time $t_{1/2}$ with methane adsorption capacity.

dependence on the pore volume (Figure 12(b)). This correlation is anticipated because the gas released in desorption canister was mainly from the adsorbed gas, instead of free gas (Figure 6).

3.4.4. Methane Adsorption Capacity. To evaluate the dependence of gas release rate on methane adsorption capacity, the variation in half-life time $t_{1/2}$ is plotted in Figure 13 as a function of methane adsorption capacity. Figure 13 shows the half-life time $t_{1/2}$ increased with an increase in methane adsorption capacity, indicating that the greater the methane adsorption capacity, the lower the gas release rate. There are two reasons for this phenomenon. First, the strong interaction between organic matter and gas molecules makes it difficult for gas molecules to desorb and transport. Second, the adsorption of methane by shale could form an adsorption layer on the pore wall, which will decrease the effective pore size and decrease the permeability, making the gas molecules difficult to transport. This phenomenon can also explain why the single-well production efficiency of coalbed gas is very low although it has much high methane adsorption capacity.

4. Conclusions

(i) Three curve patterns including L-shaped curve, S-shaped curve, and M-shaped curve are identified from the 55 two-stage gas release curves in canister

(ii) The increased temperature could significantly increase the released gas content. The released gas content shows a strong dependence on the properties that control or could increase gas adsorption and diffusion capacity, such as TOC content,

specific surface area, and permeability, while showing no dependence on the properties that control free gas storage capacity, such as inorganic minerals, porosity, and pore volume

(iii) The released gas rate shows a strong dependence on the TOC content, specific surface area, permeability, and the methane adsorption capacity, while showing no dependence on the inorganic minerals, porosity, and pore volume

Data Availability

The data used to support the findings of this study are included within the article and the supplementary materials.

Disclosure

This article acknowledges the GSA Annual Meeting in Phoenix, Arizona, USA (2019), for publishing the abstract as a poster in their conference.

Conflicts of Interest

The authors declare that the research was conducted in the absence of any commercial or financial relationships that could be construed as a potential conflict of interest.

Acknowledgments

This study was supported by the National Natural Science Foundation of China (42202175 and 41872124) and the Youth Research and Innovation Group of Xi'an Shiyou University (2019QNKYCXTD05). In addition, Prof. Jinchuan Zhang and Prof. Xuan Tang in China University of Geoscience (Beijing) are acknowledged for their insightful suggestions.

Supplementary Materials

The following are the supplementary materials related to this article. Figure S1: two-stage gas release curves of core samples from JX1 to JX32. Figure S2: two-stage gas release curves of core samples from JX33 to JX55. Table S1: experimental results of gas content for shale core samples. *(Supplementary Materials)*

References

[1] K. A. Bowker, "Barnett shale gas production, Fort Worth basin: issues and discussion," *AAPG Bulletin*, vol. 91, no. 4, pp. 523–533, 2007.

[2] C. Boyer, B. Clark, V. Jochen, R. Lewis, and C. K. Miller, "Shale gas: a global resource," *Oilfield review*, vol. 23, pp. 28–39, 2011.

[3] J. B. Curtis, "Fractured shale-gas systems," *AAPG Bulletin*, vol. 86, pp. 1921–1938, 2002.

[4] C. Sun, H. Nie, W. Dang et al., "Shale gas exploration and development in China: current status, geological challenges, and future directions," *Energy & Fuels*, vol. 35, no. 8, pp. 6359–6379, 2021.

[5] X. Tang, J. Zhang, X. Wang et al., "Shale characteristics in the southeastern Ordos basin, China: implications for hydrocarbon accumulation conditions and the potential of continental shales," *International Journal of Coal Geology*, vol. 128-129, pp. 32–46, 2014.

[6] R. Weijermars, "Economic appraisal of shale gas plays in Continental Europe," *Applied Energy*, vol. 106, pp. 100–115, 2013.

[7] J. Zhang, Z. Jin, and M. Yuan, "Reservoiring mechanism of shale gas and its distribution," *Natural Gas Industry*, vol. 24, pp. 15–18, 2004.

[8] C. Zou, D. Dong, Y. Wang et al., "Shale gas in China: characteristics, challenges and prospects (I)," *Petroleum Exploration and Development*, vol. 42, no. 6, pp. 753–767, 2015.

[9] H. Nie, P. Li, W. Dang et al., "Enrichment characteristics and exploration directions of deep shale gas of Ordovician-Silurian in the Sichuan basin and its surrounding areas, China," *Petroleum Exploration and Development*, vol. 49, no. 4, pp. 744–757, 2022.

[10] W. Dang, J. Zhang, X. Tang et al., "Investigation of gas content of organic-rich shale: a case study from Lower Permian shale in southern North China basin, Central China," *Geoscience Frontiers*, vol. 9, no. 2, pp. 559–575, 2018.

[11] Q. Meng, "Identification method for the origin of natural hydrogen gas in geological bodies," *Petroleum Geology & Experiment*, vol. 44, pp. 552–558, 2022.

[12] Q. Meng, Z. Jin, D. Sun et al., "Geological background and exploration prospects for the occurrence of high-content hydrogen," *Petroleum Geology & Experiment*, vol. 43, pp. 208–216, 2021.

[13] Q. Meng, Y. Sun, J. Tong et al., "Distribution and geochemical characteristics of hydrogen in natural gas from the Jiyang depression, eastern China," *Acta Geologica Sinica - English Edition*, vol. 89, no. 5, pp. 1616–1624, 2015.

[14] E. Shtepani, L. A. A. Noll, L. W. W. Elrod, and P. M. Jacobs, "A new regression-based method for accurate measurement of coal and shale gas content," *SPE Reservoir Evaluation & Engineering*, vol. 13, no. 2, pp. 359–364, 2010.

[15] F. Javadpour, D. Fisher, and M. Unsworth, "Nanoscale gas flow in shale gas sediments," *Journal of Canadian Petroleum Technology*, vol. 46, no. 10, p. 7, 2007.

[16] H. Nie, Z. Yang, W. Dang et al., "Study of shale gas release from freshly drilled core samples using a real-time canister monitoring technique: release kinetics, influencing factors, and upscaling," *Energy & Fuels*, vol. 34, no. 3, pp. 2916–2924, 2020.

[17] J. D. Mclennan, P. S. Schafer, T. J. Pratt, and Institute G, *A Guide to Determining Coalbed Gas Content*, Gas Research Institute, 1995.

[18] N. B. Waechter, G. L. Hampton III, and J. C. Shipps, "Overview of coal and shale gas measurement: field and laboratory procedures," in *2004 International Coalbed Methane Symposium: University of Alabama*, Tuscaloosa, Alabama, 2004.

[19] R. Cicha-Szot, L. Dudek, and P. Such, "Permeability estimation in shale formations on the basis of desorption data and radial gas flow model," *Nafta-Gaz*, vol. 71, no. 11, pp. 833–839, 2015.

[20] X. Cui, A. Bustin, and R. M. Bustin, "Measurements of gas permeability and diffusivity of tight reservoir rocks: different approaches and their applications," *Geofluids*, vol. 9, no. 3, 223 pages, 2009.

[21] F. Javadpour and A. Ettehadtavakkol, "Gas transport processes in shale," in *Fundamentals of Gas Shale Reservoirs*, pp. 245–266, John Wiley & Sons, 2015.

[22] M. A. Vasilache, "Fast and economic gas isotherm measurements using small shale samples," *Journal of Petroleum Technology*, vol. 44, pp. 1184–1190, 2010.

[23] X. Tang, Z. Jiang, S. Jiang, L. Cheng, and Y. Zhang, "Characteristics and origin of in-situ gas desorption of the Cambrian Shuijingtuo formation shale gas reservoir in the Sichuan basin, China," *Fuel*, vol. 187, pp. 285–295, 2017.

[24] H. Gao, H. Cao, and J. Zeng, "New understanding of shale gas desorption law," *Petroleum Geology and Recovery Efficiency*, vol. 26, pp. 81–86, 2019.

[25] W. Dang, J. Zhang, F. Wang, and X. Tang, "Shale gas evolution in canister: evolution characteristics, controlling factors and implications for evolved gas occurrence state," in *Abstract, GSA Annual Meeting*, Phoenix, Arizona, USA, 2019.

[26] F. Xiong, Z. Jiang, H. Huang, M. Wen, and J. Moortgat, "Mineralogy and gas content of Upper Paleozoic Shanxi and Benxi shale formations in the Ordos basin," *Energy & Fuels*, vol. 33, no. 2, pp. 1061–1068, 2019.

[27] Y. Liu, J. Zhang, and X. Tang, "Predicting the proportion of free and adsorbed gas by isotopic geochemical data: a case study from lower Permian shale in the southern North China basin (SNCB)," *International Journal of Coal Geology*, vol. 156, pp. 25–35, 2016.

[28] W. Dang, J. Zhang, X. Wei et al., "Geological controls on methane adsorption capacity of Lower Permian transitional black shales in the southern North China basin, Central China: experimental results and geological implications," *Journal of Petroleum Science and Engineering*, vol. 152, pp. 456–470, 2017.

[29] J. Tan, P. Weniger, B. Krooss et al., "Shale gas potential of the major marine shale formations in the Upper Yangtze platform, South China, part II: methane sorption capacity," *Fuel*, vol. 129, pp. 204–218, 2014.

[30] X. Tang, Z. Jiang, S. Jiang et al., "Characteristics, capability, and origin of shale gas desorption of the Longmaxi formation in the southeastern Sichuan basin, China," *Scientific Reports*, vol. 9, no. 1, p. 1035, 2019.

[31] A. Saghafi, "Determination of the gas content of coal," *Proceedings of the 16th Coal Operators' Conference*, N. Aziz and B. Kininmonth, Eds., , pp. 347–356, Mining Engineering, University of Wollongong, 2016.

[32] Y. Gensterblum, A. Ghanizadeh, R. J. Cuss et al., "Gas transport and storage capacity in shale gas reservoirs - a review. part A: transport processes," *Journal of Unconventional Oil and Gas Resources*, vol. 12, pp. 87–122, 2015.

[33] M. Holmes, D. Holmes, and A. Holmes, "A petrophysical model to estimate free gas in organic shales," in *Annual Conference and Exhibition*, Houston, Texas, 2011.

[34] S. Tang, J. Zhang, D. Elsworth et al., "Lithofacies and pore characterization of the Lower Permian Shanxi and Taiyuan shales in the southern North China Basin," *Journal of Natural Gas Science and Engineering*, vol. 36, pp. 644–661, 2016.

[35] W. Dang, H. Nie, J. Zhang et al., "Pore-scale mechanisms and characterization of light oil storage in shale nanopores: new method and insights," *Geoscience Frontiers*, vol. 13, no. 5, article 101424, 2022.

[36] P. Chareonsuppanimit, S. A. Mohammad, R. L. Robinson Jr., and K. A. Gasem, "High-pressure adsorption of gases on shales: measurements and modeling," *International Journal of Coal Geology*, vol. 95, pp. 34–46, 2012.

[37] W. Dang, J. Zhang, H. Nie et al., "Isotherms, thermodynamics and kinetics of methane-shale adsorption pair under supercritical condition: implications for understanding the nature of shale gas adsorption process," *Chemical Engineering Journal*, vol. 383, article 123191, 2020.

[38] M. Sudibandriyo, Z. Pan, J. E. Fitzgerald, R. L. Robinson, and K. A. M. Gasem, "Adsorption of methane, nitrogen, carbon dioxide, and their binary mixtures on dry activated carbon at 318.2 K and pressures up to 13.6 MPa," *Langmuir*, vol. 19, no. 13, pp. 5323–5331, 2003.

[39] I. Langmuir, "The adsorption of gases on plane surfaces of glass, mica and platinum," *Journal of the American Chemical Society*, vol. 40, no. 9, pp. 1361–1403, 1918.

[40] R. J. Ambrose, R. C. Hartman, M. Diaz Campos, I. Y. Akkutlu, and C. Sondergeld, "New pore-scale considerations for shale gas in place calculations," in *SPE Unconventional Gas Conference*, Pittsburgh, Pennsylvania, USA, 2010.

[41] C. Liu, Q. Yuan, G. Dong, Y. Liu, and J. Liu, "Optimization of fractured shale layer in Taiyuan-Shanxi formation in well ZXY1," *Sino-Global Energy*, vol. 23, pp. 32–38, 2018.

[42] R. M. Bustin, A. Bustin, D. Ross et al., "Shale gas: opportunities and challenges," *Search and Discovery*, vol. 40382, pp. 20–23, 2009.

[43] L. M. Ji, T. W. Zhang, K. L. Milliken, J. L. Qu, and X. L. Zhang, "Experimental investigation of main controls to methane adsorption in clay-rich rocks," *Applied Geochemistry*, vol. 27, no. 12, pp. 2533–2545, 2012.

[44] D. J. Ross and R. M. Bustin, "The importance of shale composition and pore structure upon gas storage potential of shale gas reservoirs," *Marine and Petroleum Geology*, vol. 26, no. 6, pp. 916–927, 2009.

[45] J. Sun, X. Xiao, Q. Wei, P. Cheng, H. Tian, and Y. Wu, "Gas in place and its controlling factors of the shallow Longmaxi shale in the Xishui area, Guizhou, China," *Journal of Natural Gas Science and Engineering*, vol. 77, article 103272, 2020.

[46] W. Dang, J. Zhang, H. Nie et al., "Microscopic occurrence characteristics of shale oil and their main controlling factors: a case study of the 3rd submember continental shale of member 7 of Yanchang formation in Yan'an area, Ordos basin," *Acta Petrolei Sinica*, vol. 43, p. 507, 2022.

[47] S. Shi, Y. Wang, Y. Sun, and H. Guo, "The volume and geochemical characteristics of desorption gases from Wufeng–Longmaxi (O_3w-S_1l) shale in the Xishui area, North Guizhou, China," *Frontiers in Earth Science*, vol. 10, article 879959, 2022.

[48] S. Schloemer and B. M. Krooss, "Molecular transport of methane, ethane and nitrogen and the influence of diffusion on the chemical and isotopic composition of natural gas accumulations," *Geofluids*, vol. 4, no. 1, 108 pages, 2004.

[49] C. Yang, J. Zhang, X. Tang et al., "Comparative study on micro-pore structure of marine, terrestrial, and transitional shales in key areas, China," *International Journal of Coal Geology*, vol. 171, pp. 76–92, 2017.

[50] J. Wang, B.'e. Wang, Y. Li, Z. Yang, H. Gong, and M. Dong, "Measurement of dynamic adsorption-diffusion process of methane in shale," *Fuel*, vol. 172, pp. 37–48, 2016.

[51] W. Dang, S. Jiang, J. Zhang et al., "Experimental and modeling study on the effect of shale composition and pressure on methane diffusivity," *Energy & Fuels*, vol. 33, no. 2, pp. 714–726, 2019.

[52] W. Dang, J. Zhang, X. Tang et al., "Shale gas potential of Lower Permian marine-continental transitional black shales in the Southern North China Basin, central China: Characterization of organic geochemistry," *Journal of Natural Gas Science and Engineering*, vol. 28, pp. 639–650, 2016.